remote sensing

MDPI

Article

Modeling the Spatial Distribution of Debris Flows and Analysis of the Controlling Factors: A Machine Learning Approach

Yan Zhao [1], Xingmin Meng [1,2,3,*], Tianjun Qi [4], Guan Chen [1], Yajun Li [1], Dongxia Yue [4] and Feng Qing [4]

[1] School of Earth Sciences, Lanzhou University, Lanzhou 730000, China; zhaoyandz@lzu.edu.cn (Y.Z.); gchen@lzu.edu.cn (G.C.); liyajun@lzu.edu.cn (Y.L.)
[2] Gansu Tech Innovation Centre for Environmental Geology and Geohazard Prevention, Lanzhou 730000, China
[3] International Science & Technology Cooperation Base for Geohazards Monitoring, Warning & Prevention, Lanzhou 730000, China
[4] College of Earth and Environmental Sciences, Lanzhou University, Lanzhou 730000, China; qitj16@lzu.edu.cn (T.Q.); dxyue@lzu.edu.cn (D.Y.); qingf16@lzu.edu.cn (F.Q.)
* Correspondence: xmmeng@lzu.edu.cn

Abstract: Debris flows are a major geological hazard in mountainous regions. For improving mitigation, it is important to study the spatial distribution and factors controlling debris flows. In the Bailong River Basin, central China, landslides and debris flows are very well developed due to the large differences in terrain, the complex geological environment, and concentrated rainfall. For analysis, 52 influencing factors, statistical, machine learning, remote sensing and GIS methods were used to analyze the spatial distribution and controlling factors of 652 debris flow catchments with different frequencies. The spatial distribution of these catchments was divided into three zones according to their differences in debris flow frequencies. A comprehensive analysis of the relationship between various factors and debris flows was made. Through parameter optimization and feature selection, the Extra Trees classifier performed the best, with an accuracy of 95.6%. The results show that lithology was the most important factor controlling debris flows in the study area (with a contribution of 26%), followed by landslide density and factors affecting slope stability (road density, fault density and peak ground acceleration, with a total contribution of 30%). The average annual frequency of daily rainfall > 20 mm was the most important triggering factor (with a contribution of 7%). Forest area and vegetation cover were also important controlling factors (with a total contribution of 9%), and they should be regarded as an important component of debris flow mitigation measures. The results are helpful to improve the understanding of factors influencing debris flows and provide a reference for the formulation of mitigation measures.

Keywords: debris flow; spatial distribution; controlling factor; machine learning

Citation: Zhao, Y.; Meng, X.; Qi, T.; Chen, G.; Li, Y.; Yue, D.; Qing, F. Modeling the Spatial Distribution of Debris Flows and Analysis of the Controlling Factors: A Machine Learning Approach. *Remote Sens.* **2021**, *13*, 4813. https://doi.org/10.3390/rs13234813

Academic Editors: Paraskevas Tsangaratos, Wei Chen and Haoyuan Hong

Received: 4 October 2021
Accepted: 25 November 2021
Published: 27 November 2021

1. Introduction

Debris flows are a major geological hazard in steep mountainous regions. They are one of the most dangerous material movements because of their high speed, long movement distance, large impact, and abruptness of onset, and for these reasons they are a major threat to life and property [1]. Therefore, it is important to determine the spatial distribution and controlling factors of debris flows in order to prevent them and mitigate their impacts [2,3].

The frequency of debris flows is mainly controlled by the coupled effects of geomorphology, material and rainfall. Many studies assumed that the material conditions were constant at the present time, and in this case the frequency of debris flows was determined entirely by the frequency of rainfall events exceeding the rainfall threshold [4–6]. However, if the rate of material supply is low, the frequency of debris flows is determined by the coupled effects of material and rainfall [3,7].

Hazard analysis of debris flows is typically conducted by establishing a relationship between their cause and occurrence [8]. Different studies have placed different emphases on the various factors influencing debris flows: e.g., geomorphic factors [9–15]; geological characteristics such as lithology and structural faults [1,2,8,16]; land cover and vegetation cover, which influence the hydrological response and the generation of debris flows [17–22]; land use [23]; climate change, such as the number of heavy rainfall events [24–26] and rainfall intensity [27,28]; landslides [29,30]; and wildfire [31]. Several studies analyzed the spatial distribution of debris flows [32–36]. In addition, landslides and rock falls induced by strong earthquakes greatly increase the number and scale of debris flows, as in the case of the 1999 Taiwan Jiji earthquake [37,38], the 2008 Wenchuan earthquake [39–42], and the 8 August 2017 Jiuzhaigou earthquake [43]. However, Dai et al. [44] confirmed that even in the presence of large quantities of debris on the slopes, the trends of landslides and debris flows seem to follow a faster recovery.

Although many studies have sought to identify the main factors controlling debris flows, it is difficult to quantitatively determine the contribution of each factor. The Bailong River Basin in central China has a complex geological environment and debris flows are extensively developed, making the area well suited to a comprehensive analysis of the various factors influencing debris flows. We used a machine learning method to model the distribution of debris flows and to quantitatively analyze their controlling factors.

2. Study Area

The Bailong River Basin is in the transition zone between the Qinghai-Tibet Plateau and the Loess Plateau, with elevations ranging from 406 to 4457 m [45]. Structurally, it is located on the eastern boundary of the Indian–Asian plate collision zone [46]. The lithology of the strata in the area is quite complicated (Figure 1). The region is strongly influenced by the Asian monsoon, with annual precipitation ranging from 300 to 900 mm; 75% of the precipitation occurs between June and September [47]. The average minimum and maximum temperatures are −14 to 3 °C in January, and 11 to 27 °C in July. As a result of large terrain differences, complex geological environments and concentrated rainfall, landslides and debris flows are very well developed [48].

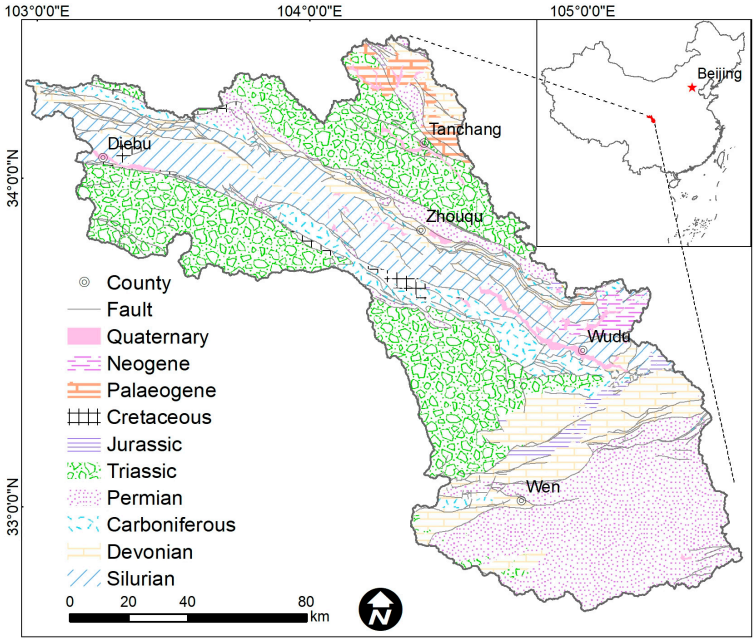

Figure 1. Geology and debris flow distribution in the Bailong River Basin.

3. Data and Methods

3.1. Debris Flow Inventory

Debris flow data were provided by the Gansu Provincial Geological Environment Monitoring Institute, which include details of the location, event time, frequency and casualties of each debris flow catchment (the starting year of the data is 2003) [1]. Combined with field surveys and a literature survey, a total of 652 debris flow catchments were obtained.

3.2. Factors Influencing Debris Flows

The formation of a debris flow is influenced by geomorphic conditions, material conditions and triggering conditions [49,50]. The parameters related to them are described below.

3.2.1. Factors Related to Geomorphic Conditions

The geomorphic characteristics of a catchment determine its gravitational potential energy conditions, water flow process [50], and hydrological characteristics [51]. (See [52] for parameter calculation methods.)

Basin area [9], main channel length [1] and curvature of the main stream [53] reflect basic information of a catchment.

The area proportions of slopes > 30°, >35°, >40°and slopes between 30° and 40° reflect the slope stability and runoff speed [54–56]. The average aspect affects the directions of water flows and soil humidity [57].

Basin relief [58], relief ratio [59] and relative relief ratio [60] reflect the gravitational potential energy condition of a catchment. Drainage density reflects the degree of drainage development [61]. Circularity ratio [62,63], form factor [61] and elongation ratio [58] reflect the basin shape.

The hypsometric integral [64] reflects the evolution of the basin geomorphology [65] and the slope distribution [13]. The Melton ratio reflects the susceptibility of debris flows [60].

Profile curvature refers to the curvature along the maximum slope direction, which affects the acceleration and deceleration of the flow, which in turn affects erosion and deposition. Plane curvature is the curvature perpendicular to the maximum slope direction, which affects the convergence and dispersion of flow.

The ruggedness number [64] is influenced positively by the structural terrain complexity [66]. The Terrain Ruggedness Index and Topographic Position Index reflect the difference between a central pixel and its surrounding cells [67].

The Topographic Wetness Index is a physically-based index or indicator of the effect of local topography on runoff flow direction and accumulation [68]. The Stream Power Index is a measure of the erosive power of flowing water [69]. The fitness ratio is the ratio of the main channel length to the basin perimeter [60].

3.2.2. Factors Related to Material Conditions

The quantity of materials and the ease with which they can be converted to a debris flow will affect its formation process, rainfall threshold and frequency.

The lithology data were divided into very hard, hard, medium, soft, and very soft according to the hardness of the rock (Table 1; Figure 2, lithology). In this study, the geological strength index (GSI) estimation was used as the estimation value of rock mass quality [70,71]. The area proportion of different hardness lithology in each catchment was calculated to analyze the influence of different lithologies on debris flows. (Lithology and fault data were obtained from a published geological map with a scale of 1: 200,000).

The linear density of faults was calculated using the line density tool in GIS software (*Fd*, Figure 2), and the average value in each catchment was determined to analyze the impact of faults on debris flows.

Table 1. Lithologies in the study area and their hardness classification.

Stratigraphic Age	Major Lithology	GSI	Relative Strength
Quaternary loose material Neogene stratified clastic rocks Paleogene stratified clastic rocks	Pebbles, gravel, silty clay Conglomerate, shale, sandstone Conglomerate	0–10	very soft
Cretaceous stratified clastic rocks	Conglomerate, sandstone, mudstone	10–20	soft
Jurassic stratified clastic rocks Silurian metamorphic rocks Devonian carbonate rocks Permian layered metamorphic rocks	Sandstone, mudstone, conglomerate, shale Sandstone, limestone, phyllite, slate Slate, phyllite, limestone Sandstone, sandy slate, tuff, phyllite	30–40	medium
Carboniferous carbonate rocks Devonian carbonate rocks Triassic and Permian layered carbonate	Limestone Limestone, shale, slate, sandstone Limestone, sandstone, shale	60–70	hard
Triassic and Permian intrusive rocks	Granite, diorite, granite gneiss, basalt, diabase	80–90	very hard

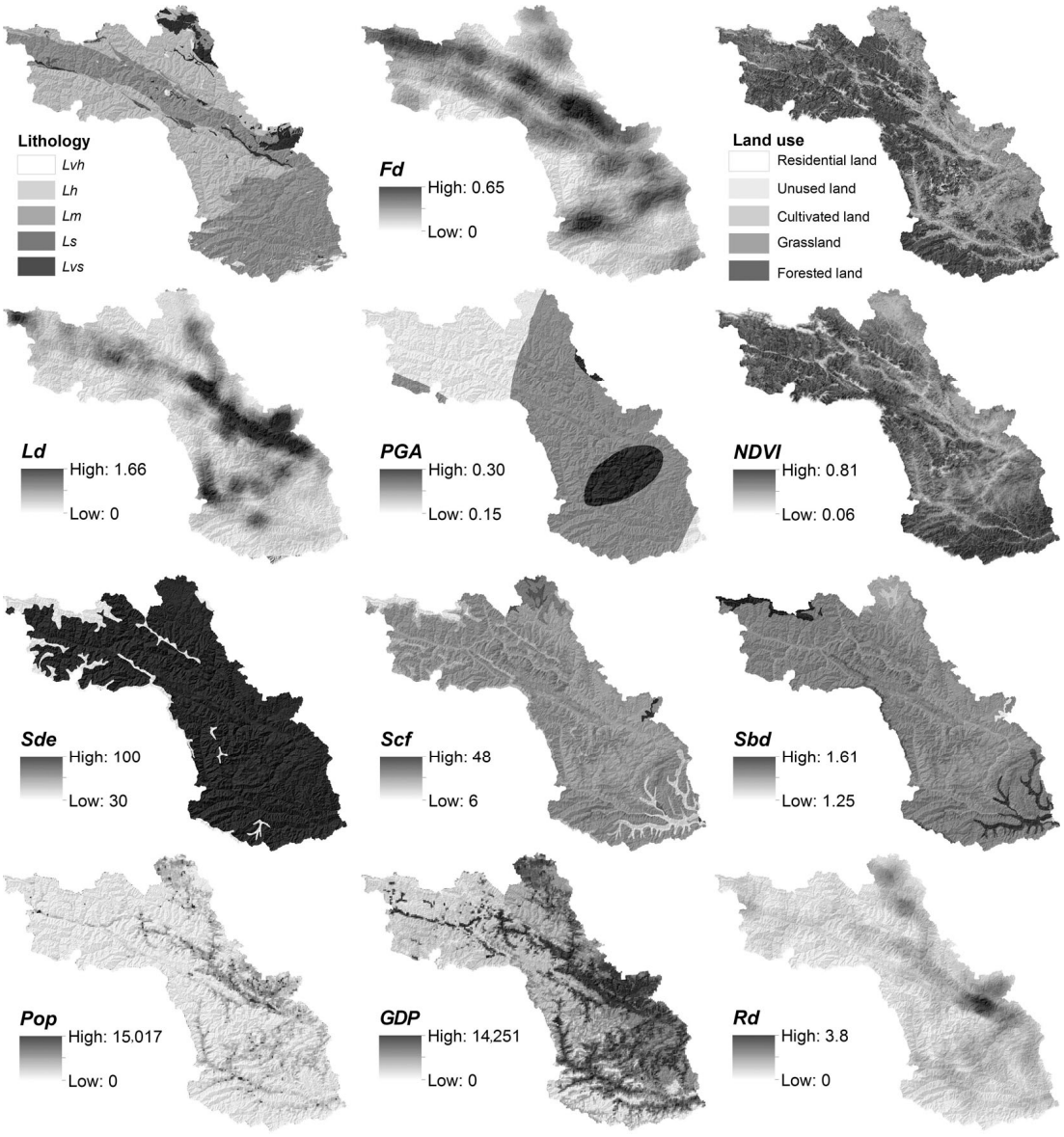

Figure 2. Distribution of factors related to material conditions.

The point density of landslides was calculated using the point density tool in GIS software (*Ld*, Figure 2), and the average value in each catchment was calculated to analyze the impact of landslides on debris flows. (The data were provided by Gansu Provincial Geological Environment Monitoring Institute).

Earthquakes affect slope stability. The average value of peak ground acceleration (*PGA*, Figure 2) in each catchment was calculated to analyze the influence of earthquakes on debris flows. (The data are from the public version of China's seismic peak ground acceleration zonation map of 2016, published by the China Seismological Bureau).

Different land use types affect surface runoff and sediment transport and may control the slope stability [2]. The area proportions of unused land, forested land, grassland, cultivated land, residential land and industrial land in each catchment were calculated to analyze the impact of different land use types on debris flows (Figure 2, Land use). (The land use data were obtained from the interpretation of remote sensing images).

The average *NDVI* (Figure 2, *NDVI*) of each catchment was calculated to analyze the impact of vegetation coverage on debris flows (*NDVI* was derived from Gaofen-1 images in August 2020).

Soil type influences rainfall runoff processes [72]. The average values of soil depth, soil clay fraction and soil bulk density in each catchment were calculated to analyze the influence of soil types on debris flows (*Sde*, *Scf* and *Sbd*, Figure 2). (Soil data were from the FAO, International Institute for Applied Systems Analysis. The soil map for China is based on Harmonized World Soil Database (HWSD, v1.1, 2009), National Tibetan Plateau Data Center, 2019).

The sum of the population and *GDP* of each catchment was calculated to reflect the impact of human activities on debris flows (*Pop* and *GDP*, Figure 2) (data source: [73]).

Roads may cut the original slopes, change the original surface confluence, and affect the slope stability. The linear density of roads was calculated (*Rd*, Figure 2), and the average value in each catchment was calculated to reflect the impact of roads on debris flows.

3.2.3. Factors Related to Triggering Conditions

Rainfall is the main triggering factor of debris flows in the study area. The average annual frequencies of daily rainfall > 15, >20, >30, >40 and >50 mm (*F15*, *F20*, *F30*, *F40* and *F50*) at each meteorological station were calculated, and Figure 3 was produced by an interpolation method. The average value of each catchment was calculated to reflect the impact of rainfall on debris flows. (The rainfall data are from 41 meteorological stations in the study area).

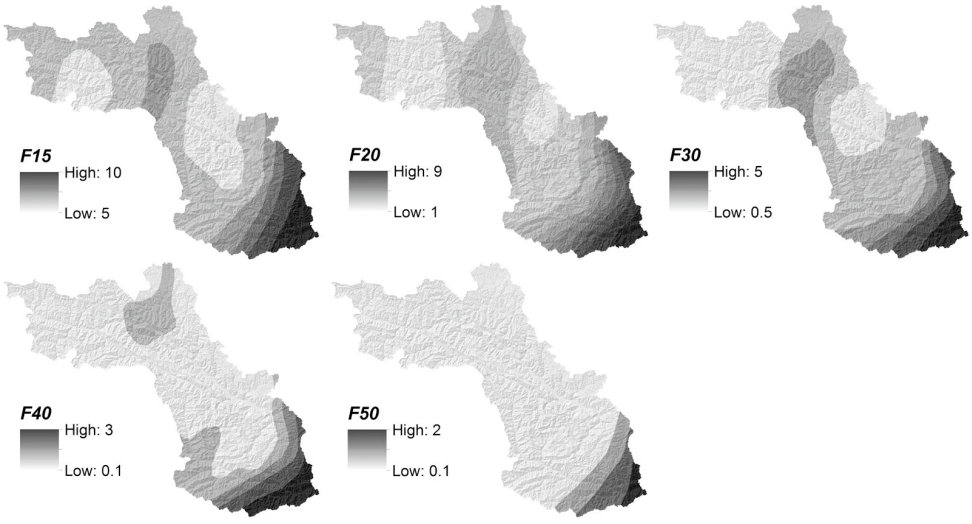

Figure 3. Distribution of factors related to triggering conditions.

Finally, a total of 52 factors influencing debris flows were selected and calculated, as shown in Table 2.

Table 2. Factors influencing debris flows. (H_{max} and H_{min} are the maximum and minimum elevations in a catchment. *Lt* is the total length of stream channels. *p* is the basin perimeter).

No.	Parameter	Abbr.	Formula	Unit
1	Basin area	*A*	GIS analysis	km^2
2	Main channel length	*Lmc*	GIS analysis	km
3	Curvature of the main stream	*Cms*	$Cms = Lmc/Ls$	/
4	Average slope	*Sa*	Average value	°
5	Area proportion of slopes > 30°	*S30*	Area of slopes > 30°/*A*	%
6	Area proportion of slopes > 35°	*S35*	Area of slopes > 35°/*A*	%
7	Area proportion of slopes > 40°	*S40*	Area of slopes > 40°/*A*	%
8	Area proportion of slopes between 30° and 40°	*S30–40*	Area of slopes 30–40°/*A*	%
9	Average aspect	*Aa*	Average value	°
10	Basin relief	*H*	$H = H_{max} - H_{min}$	km
11	Relief ratio	*Rr*	$Rr = H/L$	/
12	Relative relief ratio	*Rrr*	$Rrr = H*100/p$	/
13	Drainage density	*Dd*	$Dd = Lt/A$	/
14	Circularity ration	*Cr*	$Cr = 4\pi A/P^2$	/
15	Form factor	*Ff*	$Ff = A/L^2$	km
16	Elongation ratio	*Er*	$Er = 2\sqrt{A/\pi L^2}$	/
17	Hypsometric Integral	*HI*	$HI = (H_{mean} - H_{min})/(H_{max} - H_{min})$	/
18	Melton ratio	*Mr*	$Mr = H/\sqrt{A}$	/
19	Plane curvature	*Cpl*	GIS analysis	/
20	Profile curvature	*Cpr*	GIS analysis	/
21	Ruggedness number	*Rn*	$Rn = H*Dd$	/
22	Terrain Ruggedness Index	*TRI*	GDAL analysis	/
23	Topographic Position Index	*TPI*	GDAL analysis	/
24	Topographic Wetness Index	*TWI*	$TWI = \ln(A_s/\tan(S))$	/
25	Stream Power Index	*SPI*	$SPI = \ln(A_s*\tan(S))$	/
26	Fitness ratio	*Rf*	$Rf = Lmc/p$	/
27	Area proportion of very hard lithology	*Lvh*	Area of very hard lithology/*A*	/
28	Area proportion of hard lithology	*Lh*	Area of hard lithology/*A*	/
29	Area proportion of moderate lithology	*Lm*	Area of moderate lithology/*A*	/
30	Area proportion of soft lithology	*Ls*	Area of soft lithology/*A*	/
31	Area proportion of very soft lithology	*Lvs*	Area of very soft lithology/*A*	/
32	Fault density	*Fd*	Linear density	/
33	Area proportion of unused land	*Lun*	Area of unused land/*A*	/
34	Area proportion of forest land	*Lfo*	Area of forest land/*A*	/
35	Area proportion of grass land	*Lgr*	Area of grass land/*A*	/
36	Area proportion of cultivated land	*Lcu*	Area of cultivated land/*A*	/
37	Area proportion of residential land	*Lre*	Area of residential land/*A*	/
38	Area proportion of industrial land	*Lin*	Area of industrial land/*A*	/
39	Normalized Difference Vegetation Index	*NDVI*	Average value	/
40	Soil depth	*Sde*	Average value	cm
41	Soil clay fraction	*Scf*	Average value	%
42	Soil bulk density	*Sbd*	Average value	kg/dm^3
43	Landslide density	*Ld*	Point density	/
44	Peak ground acceleration	*PGA*	Average value	/
45	Population	*Pop*	Average value	/

Table 2. *Cont.*

No.	Parameter	Abbr.	Formula	Unit
46	Gross domestic product	*GDP*	Average value	/
47	Road density	*Rd*	Linear density	/
48	Average annual frequency of rainfall > 15 mm/d	*F15*	GIS analysis	times/yr
49	Average annual frequency of rainfall > 20 mm/d	*F20*	GIS analysis	times/yr
50	Average annual frequency of rainfall > 30 mm/d	*F30*	GIS analysis	times/yr
51	Average annual frequency of rainfall > 40 mm/d	*F40*	GIS analysis	times/yr
52	Average annual frequency of rainfall > 50 mm/d	*F50*	GIS analysis	times/yr

3.3. Machine Learning Analysis

3.3.1. Machine Learning Algorithms

Four machine learning algorithms (MLA) were selected, including Ensemble methods (Extra Trees (ETs), Gradient Boosting (GB) and Random Forest (RF)) and XGBoost (XGB). Ensemble methods combine multiple classifiers and classify new data by taking a vote of their predictions. XGBoost is a type of lifting tree model with a boosting algorithm. (See DF_distribution.ipynb for code).

3.3.2. Data Processing

Highly correlated factors may cause the instability of the models [74,75]. A cross-correlation heat map was produced (Figure 4; see features_Correlation.xlsx for details). The highly correlated factors were eliminated, including *Lmc* (0.93), *S30* (0.98), *S35* (0.96), *S40* (0.90), *TRI* (0.99), *SPI* (0.91), *Rr* (0.97), *Rrr* (0.93), *Rn* (0.89), *Er* (0.99), *F30* (0.94) and *F40* (0.89).

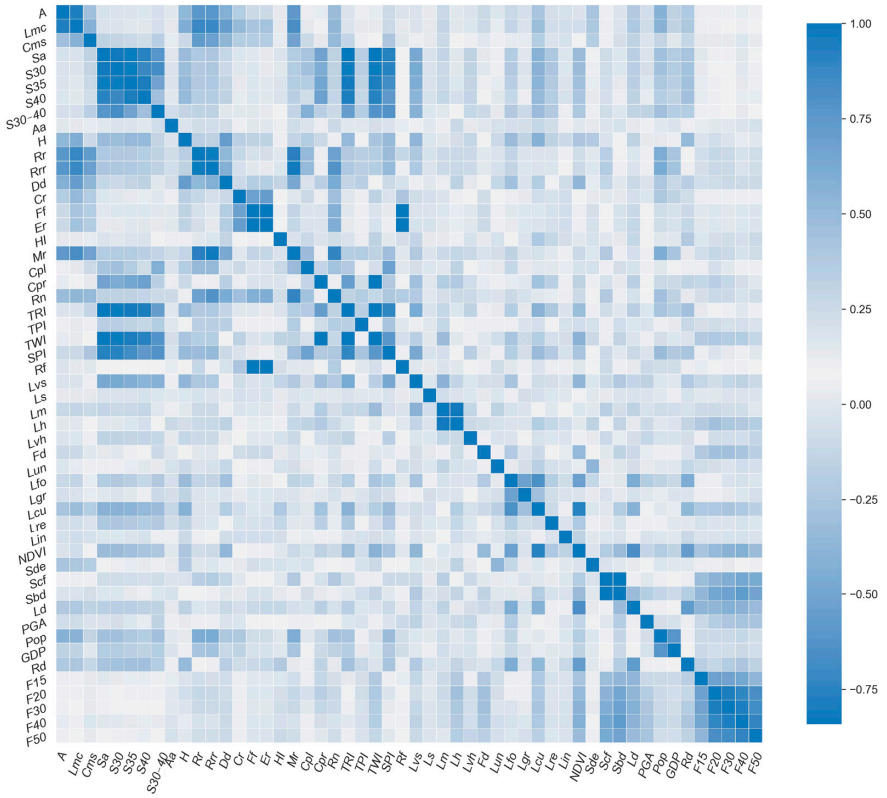

Figure 4. Cross-correlation heat map of the factors.

3.3.3. Cross−Validation

The cross−validation method was chosen to randomly select 70% of the samples for training, and the remaining 30% were used to test the model performance. This process was repeated 10 times to reduce the sampling uncertainty.

3.3.4. Model Evaluation and Optimization

The average accuracy (Acc) and standard deviation (Std) of the validation set were used to evaluate model performance. The two parameters can effectively evaluate the accuracy and stability of the models. The models were optimized by grid search for the optimal parameters. The Recursive Feature Elimination and Cross-Validation (RFECV) [76] method was used to determine the optimal number of factors.

3.3.5. Feature Importance

The feature importance method based on the mean decrease in impurity was used to calculate the importance of each factor [77]. The importance of a feature is computed as the (normalized) total reduction in the criterion brought by that feature.

4. Results

4.1. Spatial Distribution Division

The spatial distribution of 652 debris flow catchments has an obvious regularity and can be divided into three frequency zones: high zone (>2 times/year), medium zone (0.5–2 times/year) and low zone (<0.5 times/year) (Figure 5).

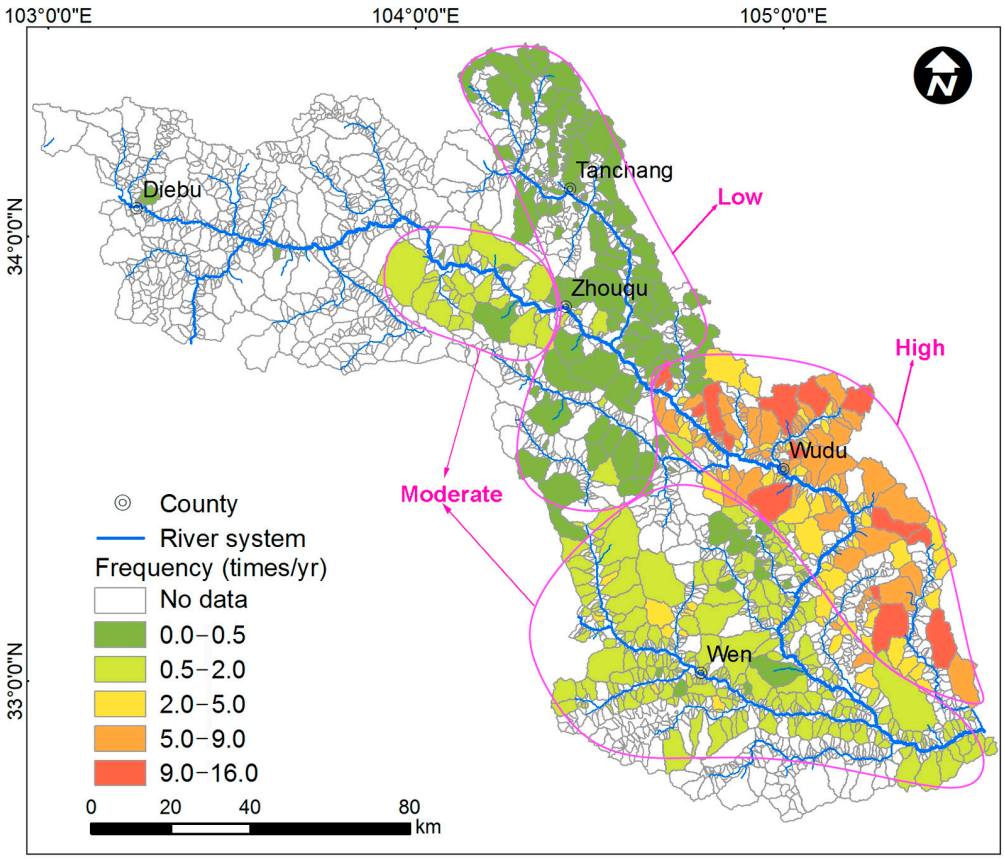

Figure 5. Frequency division results of debris flows in the Bailong River Basin.

4.2. Model Evaluation and Optimization

After modeling and parameter optimization, the optimal parameters and the Acc of the validation set are listed in Table 3. The results show that the ETs performed the best and hence was selected for further optimization. The optimal number of factors of ETs was determined using RFECV (Table 4). It can be seen that the number of factors was reduced from 40 to 18, and the Acc of the models had been slightly improved. The final Acc of ETs is 95.6%, indicating that the model can correctly judge which frequency zone most catchments belong to.

Table 3. Optimization results of models.

MLA	Optimal Parameter	Acc	Std
ETS	*n*_estimators = 200; max_depth = 22; criterion = entropy	0.952	0.0166
XGB	*n*_estimators = 50; learning_rate = 0.25; max_depth = 6	0.948	0.0153
GB	*n*_estimators = 50; learning_rate = 0.25; criterion = friedman_mse; max_depth = 6	0.947	0.0173
RF	*n*_estimators = 500; criterion = gini; oob_score = True; max_depth = 14	0.936	0.0169

Table 4. Feature selection results of ETs.

	Acc	Std	Factors	Number
Before RFECV	0.952	0.0166	*A*, *Cms*, *Sa*, *S30–40*, *Aa*, *H*, *Dd*, *Cr*, *Ff*, *HI*, *Mr*, *Cpl*, *Cpr*, *TPI*, *TWI*, *Rf*, *Lvs*, *Ls*, *Lm*, *Lh*, *Lvh*, *Fd*, *Lun*, *Lfo*, *Lgr*, *Lcu*, *Lre*, *Lin*, *NDVI*, *Sde*, *Scf*, *Sbd*, *Ld*, *PGA*, *Pop*, *GDP*, *Rd*, *F15*, *F20*, *F50*	40
After RFECV	0.956	0.0149	*Sa*, *Mr*, *Cpl*, *Cpr*, *Lvs*, *Lm*, *Lh*, *Fd*, *Lfo*, *Lgr*, *Lcu*, *NDVI*, *Sbd*, *Ld*, *PGA*, *Rd*, *F15*, *F20*	18

4.3. Importance of the Factors

The importance scores of 18 factors were calculated (Figure 6). It can be seen that the most important factor is lithology, including *Lm* (with a contribution of 13%), *Lh* (with a contribution of 8%) and *Lvs* (with a contribution of 5%). The second most important factors are landslide density (*Ld*, with a contribution of 10%) and road density (*Rd*, with a contribution of 10%), flowed by fault density (*Fd*, with a contribution of 5%) and peak ground acceleration (*PGA*, with a contribution of 5%). The average annual frequency of daily rainfall > 20 mm (*F20*, with a contribution of 7%) is the most important triggering condition of debris flows. The area proportion of forest land (*Lfo*, with a contribution of 5%) and vegetation cover (*NDVI*, with a contribution of 4%) are also important factors controlling debris flows in the study area.

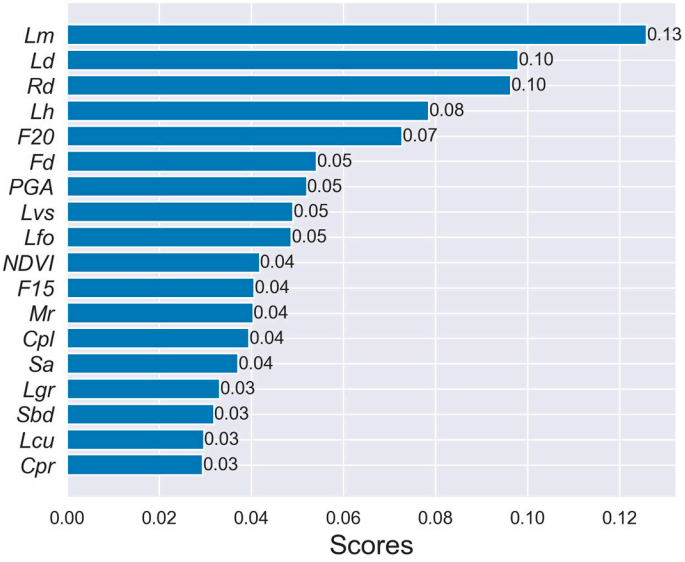

Figure 6. Importance ranking of factors.

5. Discussion

5.1. Spatial Distribution and Influencing Factors

The spatial distribution of 652 debris flow catchments was divided into three zones according to their differences in debris flow frequencies. Such typical regional distribution characteristics are suitable for a comprehensive analysis of the relationship between various factors and debris flows.

In order to analyze the distribution characteristics of various factors, a box plot of each factor in the high, moderate and low zones were produced in Figure 7. The high zone and moderate zone have similar high rainfall conditions (*F15*, *F20*, *F50*), and the moderate zone has more favorable geomorphic conditions (higher *Sa*, *S30*, *S30–40*, *H*, *Ff*, *HI* and *Mr*). However, debris flow frequency in the moderate zone is lower than in the high zone, which indicates that the difference between them is mainly caused by material conditions. Compared with the moderate zone, the high zone has more favorable material supply conditions (higher *Fd*, *Ld* and *Lvs*), and is more affected by human activities (higher *Rd*, *Lcu* and *Pop*). In addition, the moderate zone has a higher vegetation coverage (higher *Lfo* and *NDVI*). Therefore, the high zone has a higher debris flow frequency.

Compared with the high and moderate zones, the low zone has less favorable rainfall conditions (lower *F15*, *F20*, *F30* and *F40*), material supply conditions (lower *Lh*), and geomorphic conditions (lower *Sa*, *H*, *Dd* and *Mr*). The other factors for the low zone are generally intermediate between the high and moderate zones. Therefore, the low zone has the lowest debris flow frequency.

In summary, the conditions of more favorable rainfall and material supply and more intensive human activities are responsible for the high debris flow frequency in the high zone. Under similar rainfall conditions with the high zone, a lower material supply, less intense human activities, and higher forest cover are responsible for the moderate debris flow frequency in the moderate zone. The less favorable rainfall, material supply and geomorphic conditions are responsible for the lowest debris flow frequency in the low zone.

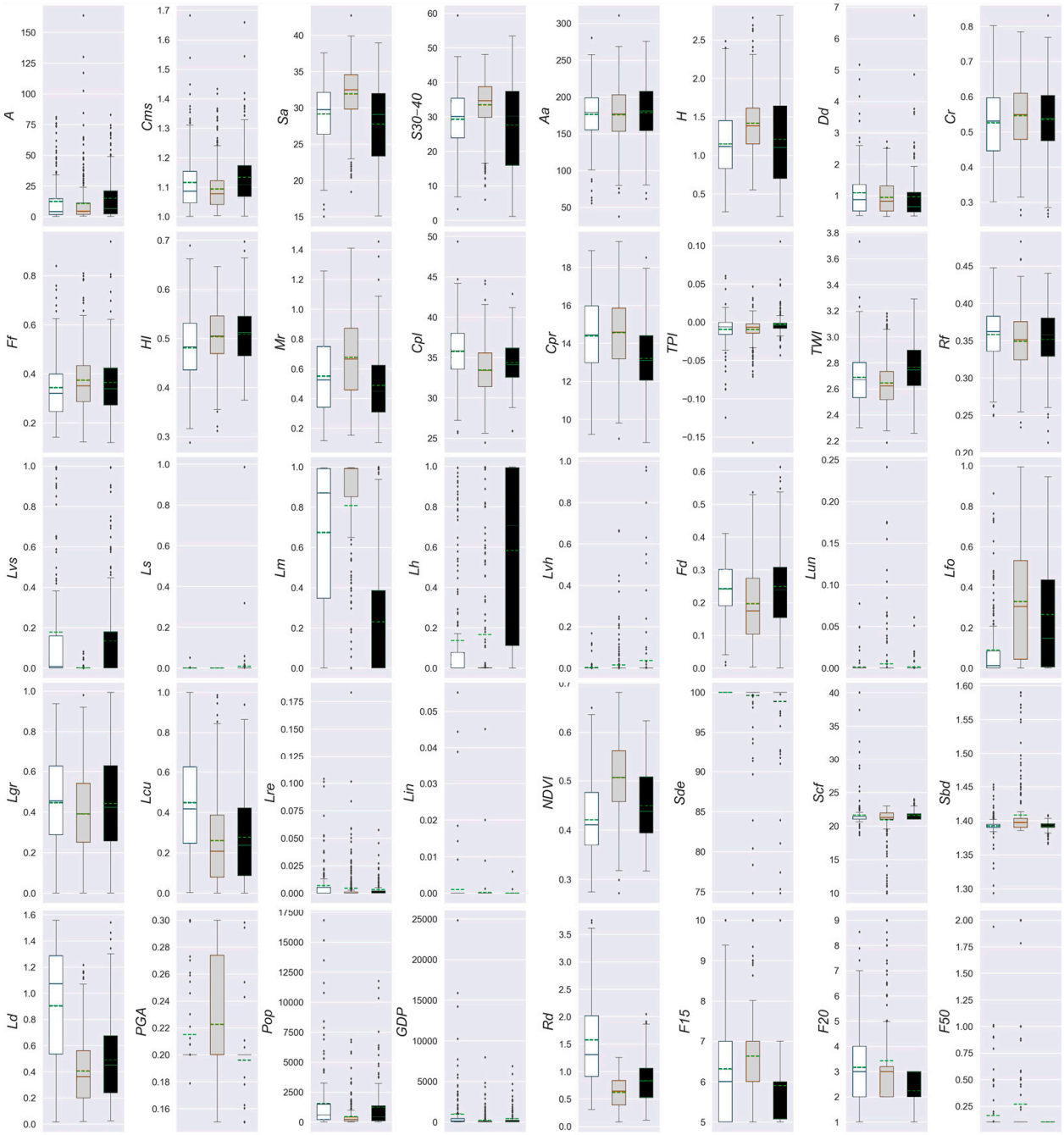

Figure 7. Box plots of the factors in different debris flow frequency zones. (White indicates the high zone; grey indicates the moderate zone; and black indicates the low zone).

5.2. Feature Importance Analysis

The importance of factors in Figure 6 shows that lithologies (with a total contribution of 26%) control the main distribution of debris flow catchments in the study area. Many studies showed that lithology was an important factor controlling the spatial distribution of debris flows [1,2] and affecting the supply of loose debris [78]. Our study quantitatively calculates the contribution of different lithologies to the spatial distribution of debris flows, and we can better understand the relationship between lithology distribution and debris flows. Figure 8 (Lithology) shows that the high zone is mainly distributed in *Lvs* and *Lm* areas, the moderate zone is mainly distributed in *Lm* areas, and the low zone is mainly distributed in *Lh* areas.

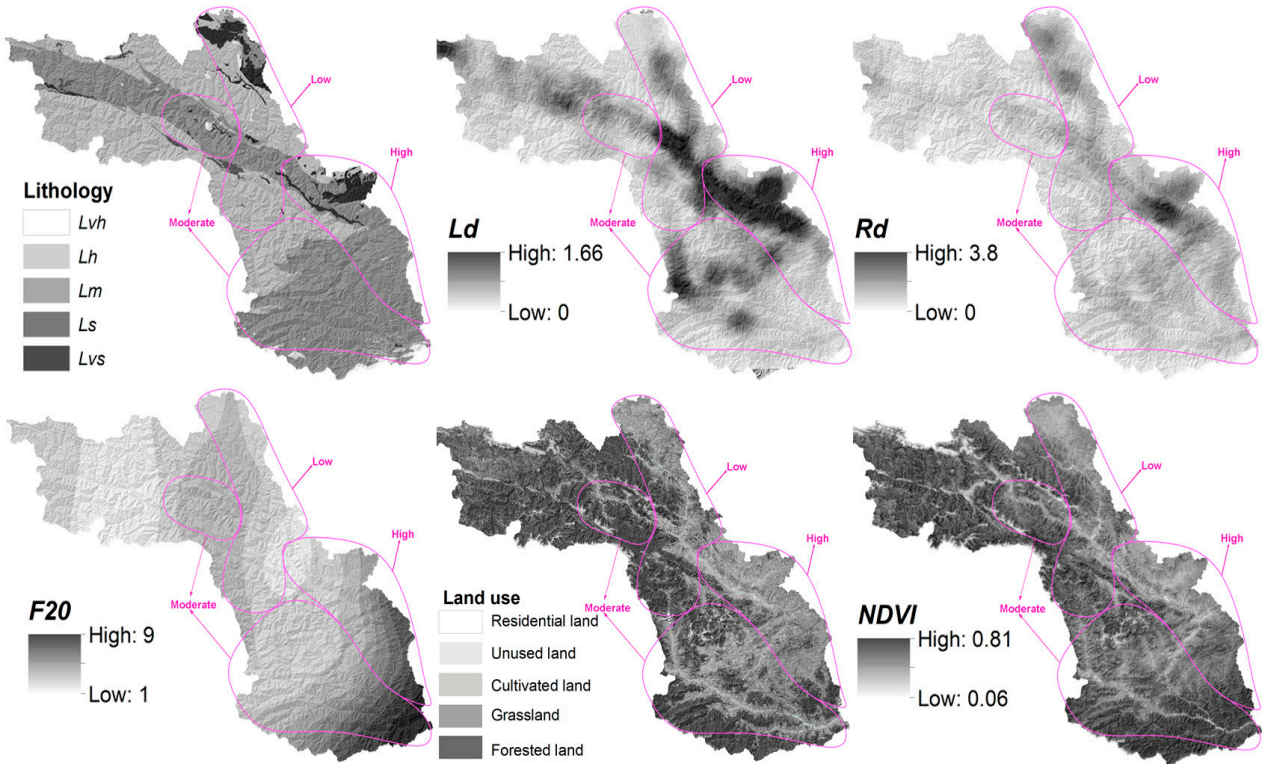

Figure 8. Distribution of important factors.

The second most important factor is landslide density (*Ld*, with a contribution of 10%). Many studies showed that the frequency of debris flows would increase significantly within 1–8 years after a large landslide [30]. Landslides and rock falls caused by an earthquake would reduce rainfall thresholds of debris flows and increase the number and scale of debris flows [38–40,43]. However, some studies indicated that there was no direct relationship between landslide distribution and debris flows [79], and coseismic landslide was not the main material source driving debris flows after an earthquake [20], so landslides need a certain process to mobilize to form debris flows [80].

Road density (*Rd*, with a contribution of 10%) mainly reflects the influence of human activities on slope stability. Fault density (*Fd*, with a contribution of 5%) and peak ground acceleration (*PGA*, with a contribution of 5%) also affect the slope stability. This is an important reason for the significant decrease in the rainfall threshold of debris flows after an earthquake.

The average annual frequency of daily rainfall > 20 mm (*F20*, with a contribution of 7%) is also an important factor. The high and moderate zones are mainly distributed in the areas with higher *F20*, and the low zone is mainly distributed in the areas with lower *F20*.

The area proportion of forest and vegetation cover are also important factors (with a total contribution of 9%), which gives us a new understanding of the role of vegetation in reducing debris flows. Forest cover mainly reduces the supply of loose materials and slows down the confluence speed [81–83]. Comparison of the high and moderate zones indicates that, even if the moderate zone has more favorable geomorphic conditions (higher *Sa*, *S30*, *S30–40*, *H*, *Ff*, *HI* and *Mr*) and precipitation conditions (Figure 8, *F20*), but the material conditions are less favorable than the high zone (Figure 8, *Ld*, *Rd* and Lithology), and the vegetation cover (especially forest cover) is higher than the high zone (Figure 8, Land use and *NDVI*), the result is lower debris flow frequency in the moderate zone. This is consistent with the results of Guo et al. [20], who found that a lower material supply and higher vegetation coverage can effectively reduce the frequency of debris flows and increase the rainfall threshold. Therefore, vegetation cover, especially forest cover, is an important factor to be considered when formulating debris flow mitigation measures [84–86].

It appears that factors related to geomorphology have little influence on debris flows in the study area. One of the most important factors is the Melton ratio (*Mr*), which may be because the terrain difference in the study area is generally large and there is little differentiation.

Among the important factors, except for the vegetation coverage and the proportion of forest, another factor that can be readily controlled is the road density. Reducing road construction can reduce the material supply on unstable slopes to debris flows. However, it would potentially impact the economic development of the region and would require careful evaluation by decision makers.

The contribution of this section is to quantitatively evaluate the importance of each factor for the spatial distribution of debris flows, which helps us better understand their relationship. Through the above analysis, we have a new understanding of the factors influencing the spatial distribution of debris flows, which has reference value for better formulating disaster reduction measures.

5.3. Estimation of Daily Rainfall Threshold

The average annual frequencies of daily rainfall >15, >20, >30, >20, >40 and >50 mm in each zone were determined in Table 5. Taking the daily rainfall with the average annual rainfall frequencies equal to the debris flow frequencies as the daily rainfall threshold, the daily rainfall threshold is ~15–30 mm in the high zone, ~30–40 mm in the moderate zone, and >40 mm in the low zone. The daily rainfall thresholds can provide a reference for regional debris flow early warning.

Table 5. Debris flow frequencies and average annual frequencies of daily rainfall >15, >20, >30, >40 and >50 mm in different zones (times/year).

Zone	Debris Flow Frequency	>15 mm	>20 mm	>30 mm	>40 mm	>50 mm
High	>2	5–9.5	1–7	1–2	<0.5	<0.25
Moderate	0.5–2	5–8	2–5	1–3	0.3–1	<0.25
Low	<0.5	5–7	1–3	0.5–1.5	<0.5	<0.25

5.4. Uncertainties

The data used in this paper includes detailed investigation data (debris flow inventory) and the data obtained from public websites (DEM, remote sensing images, geological data, soil data, population, GDP, road and rainfall), which ensure the quality of the data. However, compiling data related to debris flows is challenging. Therefore, like other related studies, our study had some uncertainties due to the influence of the amount and quality of available data.

6. Conclusions

The main contribution of this study has been to analyze and model the spatial distribution of debris flows with different frequencies in the Bailong River Basin, central China, where debris flows are very well developed. To do this, we divided 652 debris flow catchments into three frequency zones and analyzed a comprehensive range of factors using statistical and machine learning methods. The factors controlling the distribution of debris flows were analyzed quantitatively. The results potentially provide a deeper understanding of factors controlling debris flows and have an important reference value for formulating debris flow mitigation measures. The major findings are summarized below.

1. The main factor controlling debris flows in the study area is lithology. The medium, hard and very soft lithologies control the major distribution of debris flow catchments.
2. Landslides and the factors affecting slope stability (including roads, faults and earthquakes) are the second most important factors. The factor that can be easily controlled

is road construction, although controlling this may adversely affect regional economic development.
3. The most important triggering factor of debris flows is the average annual frequency of daily rainfall >20 mm. We also estimated the daily rainfall thresholds of debris flows in different zones.
4. The area proportion of forest and vegetation cover are also important factors controlling debris flows, which can be an important part of debris flow mitigation measures.

Author Contributions: Conceptualization, methodology, software, writing—original draft preparation, Y.Z.; supervision, validation, resources, X.M. and G.C.; visualization, investigation, data curation, T.Q., Y.L. and F.Q.; writing—reviewing and editing, D.Y. All authors have read and agreed to publish the version of the manuscript.

Funding: This work was supported by the National Key Research and Development Program of China (2017YFC1501005, 2018YFC1504704); the Major Scientific and Technological Projects of Gansu Province (19ZD2FA002); the National Natural Science Foundation of China (42130709, 41907224); the Program for International S&T Cooperation Projects of Gansu Province (2018−0204−GJC−0043); the Natural Science Foundation of Gansu Province (21JR7RA442); and the Construction Project of Gansu Technological Innovation Center (18JR2JA006).

Data Availability Statement: The data and code used in this paper are available at: http://dx.doi.org/10.13140/RG.2.2.11129.19048 [87].

Acknowledgments: The DEM data were provided by the International Scientific and Technical Data Mirror Site, Computer Network Information Center, Chinese Academy of Sciences.

Conflicts of Interest: The authors declare no conflict of interest.

References

1. Zhao, Y.; Meng, X.; Qi, T.; Qing, F.; Xiong, M.; Li, Y.; Guo, P.; Chen, G. AI-based identification of low-frequency debris flow catchments in the Bailong River basin, China. *Geomorphology* **2020**, *359*, 107125. [CrossRef]
2. Jomelli, V.; Pavlova, I.; Giacona, F.; Zgheib, T.; Eckert, N. Respective influence of geomorphologic and climate conditions on debris-flow occurrence in the Northern French Alps. *Landslides* **2019**, *16*, 1871–1883. [CrossRef]
3. Jakob, M.; Bovis, M.; Oden, M. The significance of channel recharge rates for estimating debris-flow magnitude and frequency. *Earth Surf. Process. Landf.* **2005**, *30*, 755–766. [CrossRef]
4. Zimmermann, M.; Haeberli, W. Climatic change and debris flow activity in high-mountain areas—A case study in the Swiss Alps. *Catena Suppl.* **1992**, *22*, 59–72.
5. Zimmermann, M.; Mani, P.; Romang, H. Magnitude-frequency aspects of alpine debris flows. *Eclogae Geol. Helv.* **1997**, *90*, 415–420. [CrossRef]
6. Bovis, M.J.; Jakob, M. The role of debris supply conditions in predicting debris flow activity. *Earth Surf. Process. Landf.* **1999**, *24*, 1039–1054. [CrossRef]
7. Glade, T. Linking debris-flow hazard assessments with geomorphology. *Geomorphology* **2005**, *66*, 189–213. [CrossRef]
8. Cheng, W.; Wang, N.; Zhao, M.; Zhao, S. Relative tectonics and debris flow hazards in the Beijing mountain area from DEM-derived geomorphic indices and drainage analysis. *Geomorphology* **2016**, *257*, 134–142. [CrossRef]
9. Chang, T.C.; Chao, R.J. Application of back-propagation networks in debris flow prediction. *Eng. Geol.* **2006**, *85*, 270–280. [CrossRef]
10. Kovanen, D.J.; Slaymaker, O. The morphometric and stratigraphic framework for estimates of debris flow incidence in the North Cascades foothills, Washington State, USA. *Geomorphology* **2008**, *99*, 224–245. [CrossRef]
11. Bertrand, M.; Liébault, F.; Piégay, H. Debris-flow susceptibility of upland catchments. *Nat. Hazards* **2013**, *67*, 497–511. [CrossRef]
12. Liu, J.J.; Li, Y.; Su, P.C.; Cheng, Z.L. Magnitude–frequency relations in debris flow. *Environ. Geol.* **2008**, *55*, 1345–1354. [CrossRef]
13. Johnson, P.A.; McCuen, R.H.; Hromadka, T.V. Magnitude and frequency of debris flows. *J. Hydrol.* **1991**, *123*, 69–82. [CrossRef]
14. Qing, F.; Zhao, Y.; Meng, X.; Su, X.; Qi, T.; Yue, D. Application of Machine Learning to Debris Flow Susceptibility Mapping along the China–Pakistan Karakoram Highway. *Remote Sens.* **2020**, *12*, 2933. [CrossRef]
15. Qi, T.; Zhao, Y.; Meng, X.; Chen, G.; Dijkstra, T. AI-Based Susceptibility Analysis of Shallow Landslides Induced by Heavy Rainfall in Tianshui, China. *Remote Sens.* **2021**, *13*, 1819. [CrossRef]
16. Esper Angillieri, M.Y. Debris flow susceptibility mapping using frequency ratio and seed cells, in a portion of a mountain international route, Dry Central Andes of Argentina. *Catena* **2020**, *189*, 104504. [CrossRef]
17. Imaizumi, F.; Sidle, R.C.; Kamei, R. Effects of forest harvesting on the occurrence of landslides and debris flows in steep terrain of central Japan. *Earth Surf. Process. Landf.* **2008**, *33*, 827–840. [CrossRef]

18. Ghestem, M.; Veylon, G.; Bernard, A.; Vanel, Q.; Stokes, A. Influence of plant root system morphology and architectural traits on soil shear resistance. *Plant Soil* **2014**, *377*, 43–61. [CrossRef]
19. Winter, M.G.; Smith, J.T.; Fotopoulou, S.; Pitilakis, K.; Mavrouli, O.; Corominas, J.; Argyroudis, S. An expert judgement approach to determining the physical vulnerability of roads to debris flow. *Bull. Eng. Geol. Environ.* **2014**, *73*, 291–305. [CrossRef]
20. Guo, X.; Chen, X.; Song, G.; Zhuang, J.; Fan, J. Debris flows in the Lushan earthquake area: Formation characteristics, rainfall conditions, and evolutionary tendency. *Nat. Hazards* **2021**, *106*, 2663–2687. [CrossRef]
21. Rengers, F.K.; McGuire, L.A.; Coe, J.A.; Kean, J.W.; Baum, R.L.; Staley, D.M.; Godt, J.W. The influence of vegetation on debris-flow initiation during extreme rainfall in the northern Colorado Front Range. *Geology* **2016**, *44*, 823–826. [CrossRef]
22. Rogelis, M.C.; Werner, M. Regional debris flow susceptibility analysis in mountainous peri-urban areas through morphometric and land cover indicators. *Nat. Hazards Earth Syst. Sci.* **2014**, *14*, 3043–3064. [CrossRef]
23. Lorente, A.; García-Ruiz, J.M.; Beguería, S.; Arnáez, J. Factors explaining the spatial distribution of hillslope debris flows: A case study in the Flysch Sector of the Central Spanish Pyrenees. *Mt. Res. Dev.* **2002**, *22*, 32–39. [CrossRef]
24. Jomelli, V.; Pech, V.P.; Chochillon, C.; Brunstein, D. Geomorphic Variations of Debris Flows and Recent Climatic Change in the French Alps. *Clim. Chang.* **2004**, *64*, 77–102. [CrossRef]
25. Jomelli, V.; Brunstein, D.; Grancher, D.; Pech, P. Is the response of hill slope debris flows to recent climate change univocal? A case study in the Massif des Ecrins (French Alps). *Clim. Chang.* **2007**, *85*, 119–137. [CrossRef]
26. Kean, J.W.; Staley, D.M. Forecasting the Frequency and Magnitude of Postfire Debris Flows Across Southern California. *Earth's Future* **2021**, *9*, e2020EF001735. [CrossRef]
27. Pelfini, M.; Santilli, M. Frequency of debris flows and their relation with precipitation: A case study in the Central Alps, Italy. *Geomorphology* **2008**, *101*, 721–730. [CrossRef]
28. Van Steijn, H. Debris-flow magnitude—frequency relationships for mountainous regions of Central and Northwest Europe. *Geomorphology* **1996**, *15*, 259–273. [CrossRef]
29. Frank, F.; McArdell, B.W.; Huggel, C.; Vieli, A. The importance of entrainment and bulking on debris flow runout modeling: Examples from the Swiss Alps. *Nat. Hazards Earth Syst. Sci.* **2015**, *15*, 2569–2583. [CrossRef]
30. Frank, F.; Huggel, C.; McArdell, B.W.; Vieli, A. Landslides and increased debris-flow activity: A systematic comparison of six catchments in Switzerland. *Earth Surf. Process. Landf.* **2019**, *44*, 699–712. [CrossRef]
31. Kern, A.N.; Addison, P.; Oommen, T.; Salazar, S.E.; Coffman, R.A. Machine Learning Based Predictive Modeling of Debris Flow Probability Following Wildfire in the Intermountain Western United States. *Math. Geosci.* **2017**, *49*, 717–735. [CrossRef]
32. Wieczorek, G.F.; Harp, E.L.; Mark, R.K.; Bhattacharyya, A.K. Debris flows and other landslides in San Mateo, Santa Cruz, Contra Costa, Alameda, Napa, Solano, Sonoma, Lake, and Yolo Counties, and factors influencing debris-flow distribution. In Proceedings of the Landslides, Floods, and Marine Effects of the Storm, San Francisco Bay region, CA, USA, 3–5 January 1982; U.S. Geological Survey: Reston, VA, USA, 1988; pp. 133–162.
33. He, Y.P.; Chen, J.; Li, Y.; Cui, P. Debris-flow distribution and hazards along the Sichuan-Tibet and Sino-Nepal highway, Tibet, China. In *Proceedings of the 3rd International Conference on Debris-Flow Hazards Mitigation: Mechanics, Prediction, and Assessment*; Millpress Sciences Publishers: Davos, Switzerland, 2003; Volume 2, pp. 955–964.
34. Wieczorek, G.F.; Mossa, G.S.; Morgan, B.A. Regional debris-flow distribution and preliminary risk assessment from severe storm events in the Appalachian Blue Ridge Province, USA. *Landslides* **2004**, *1*, 53–59. [CrossRef]
35. Wei, F.; Jiang, Y.; Zhao, Y.; Xu, A.; Gardner, J.S. The distribution of debris flows and debris flow hazards in southeast China. In *Monitoring, Simulation, Prevention and Remediation of Dense and Debris Flows III*; Wessex Institute of Technology Press: Ashurst, UK, 2010; Volume 67, pp. 137–147.
36. He, N.; Chen, N.S. Study on China's Debris Flow Distribution and Occurrence Trend. *Appl. Mech. Mater.* **2012**, *204–208*, 3345–3350. [CrossRef]
37. Lin, C.-W.; Liu, S.-H.; Lee, S.-Y.; Liu, C.-C. Impacts of the Chi-Chi earthquake on subsequent rainfall-induced landslides in central Taiwan. *Eng. Geol.* **2006**, *86*, 87–101. [CrossRef]
38. Lin, C.W.; Shieh, C.L.; Yuan, B.D.; Shieh, Y.C.; Liu, S.H.; Lee, S.Y. Impact of Chi-Chi earthquake on the occurrence of landslides and debris flows: Example from the Chenyulan River watershed, Nantou, Taiwan. *Eng. Geol.* **2004**, *71*, 49–61. [CrossRef]
39. Tang, C.; Zhu, J.; Li, W.L.; Liang, J.T. Rainfall-triggered debris flows following the Wenchuan earthquake. *Bull. Eng. Geol. Environ.* **2009**, *68*, 187–194. [CrossRef]
40. Cui, P.; Chen, X.Q.; Zhu, Y.Y.; Su, F.H.; Wei, F.Q.; Han, Y.S.; Liu, H.J.; Zhuang, J.Q. The Wenchuan Earthquake (May 12, 2008), Sichuan Province, China, and resulting geohazards. *Nat. Hazards* **2011**, *56*, 19–36. [CrossRef]
41. Huang, R.; Fan, X. The landslide story. *Nat. Geosci.* **2013**, *6*, 325–326. [CrossRef]
42. Fan, X.; Scaringi, G.; Korup, O.; West, A.J.; Westen, C.J.; Tanyas, H.; Hovius, N.; Hales, T.C.; Jibson, R.W.; Allstadt, K.E.; et al. Earthquake-Induced Chains of Geologic Hazards: Patterns, Mechanisms, and Impacts. *Rev. Geophys.* **2019**, *57*, 421–503. [CrossRef]
43. Hu, X.; Hu, K.; Tang, J.; You, Y.; Wu, C. Assessment of debris-flow potential dangers in the Jiuzhaigou Valley following the August 8, 2017, Jiuzhaigou earthquake, western China. *Eng. Geol.* **2019**, *256*, 57–66. [CrossRef]
44. Dai, L.; Scaringi, G.; Fan, X.; Yunus, A.P.; Liu-Zeng, J.; Xu, Q.; Huang, R. Coseismic Debris Remains in the Orogen Despite a Decade of Enhanced Landsliding. *Geophys. Res. Lett.* **2021**, *48*, e2021GL095850. [CrossRef]
45. Zhao, Y.; Meng, X.; Qi, T.; Li, Y.; Chen, G.; Yue, D.; Qing, F. AI-based rainfall prediction model for debris flows. *Eng. Geol.* **2021**, 106456. [CrossRef]

46. Qi, T.; Meng, X.; Qing, F.; Zhao, Y.; Shi, W.; Chen, G.; Zhang, Y.; Li, Y.; Yue, D.; Su, X.; et al. Distribution and characteristics of large landslides in a fault zone: A case study of the NE Qinghai-Tibet Plateau. *Geomorphology* **2021**, *379*, 107592. [CrossRef]
47. Xiong, M.; Meng, X.; Wang, S.; Guo, P.; Li, Y.; Chen, G.; Qing, F.; Cui, Z.; Zhao, Y. Effectiveness of debris flow mitigation strategies in mountainous regions. *Prog. Phys. Geogr.* **2016**, *40*, 768–793. [CrossRef]
48. Tang, C.; Rengers, N.; van Asch, T.W.J.; Yang, Y.H.; Wang, G.F. Triggering conditions and depositional characteristics of a disastrous debris flow event in Zhouqu city, Gansu Province, northwestern China. *Nat. Hazards Earth Syst. Sci.* **2011**, *11*, 2903–2912. [CrossRef]
49. Iverson, R.M. The physics of debris flows. *Rev. Geophys.* **1997**, *35*, 245–296. [CrossRef]
50. Wei, F.; Gao, K.; Hu, K.; Li, Y.; Gardner, J.S. Relationships between debris flows and earth surface factors in Southwest China. *Environ. Geol.* **2008**, *55*, 619–627. [CrossRef]
51. Singh, P.; Thakur, J.K.; Singh, U.C. Morphometric analysis of Morar River Basin, Madhya Pradesh, India, using remote sensing and GIS techniques. *Environ. Earth Sci.* **2013**, *68*, 1967–1977. [CrossRef]
52. Zhao, Y. Calculation Methods of Commonly Used Basin Geomorphological Parameters. Available online: http://dx.doi.org/10.13140/RG.2.2.12459.77605/3 (accessed on 20 November 2021).
53. Li, Y.; Wang, H.; Chen, J.; Shang, Y. Debris Flow Susceptibility Assessment in the Wudongde Dam Area, China Based on Rock Engineering System and Fuzzy C-Means Algorithm. *Water* **2017**, *9*, 669. [CrossRef]
54. Stevaux, J.C.; de Azevedo Macedo, H.; Assine, M.L.; Silva, A. Changing fluvial styles and backwater flooding along the Upper Paraguay River plains in the Brazilian Pantanal wetland. *Geomorphology* **2020**, *350*, 106906. [CrossRef]
55. Wilford, D.J.; Sakals, M.E.; Innes, J.L.; Sidle, R.C.; Bergerud, W.A. Recognition of debris flow, debris flood and flood hazard through watershed morphometrics. *Landslides* **2004**, *1*, 61–66. [CrossRef]
56. Zhou, W.; Tang, C.; Van Asch, T.W.J.; Chang, M. A rapid method to identify the potential of debris flow development induced by rainfall in the catchments of the Wenchuan earthquake area. *Landslides* **2016**, *13*, 1243–1259. [CrossRef]
57. Chu, H.; Wu, W.; Wang, Q.J.; Nathan, R.; Wei, J. An ANN-based emulation modelling framework for flood inundation modelling: Application, challenges and future directions. *Environ. Model. Softw.* **2020**, *124*, 104587. [CrossRef]
58. Schumm, S.A. Evolution of drainage systems and slopes in badlands at Perth Amboy, New Jersey. *Bull. Geol. Soc. Am.* **1956**, *67*, 597–646. [CrossRef]
59. Schumm, S.A. The relation of drainage basin relief to sediment loss. In *Proceedings of the International Union Geodesy Geophysics, 10th General Assembly (Rome)*; International Association of Scientific Hydrology: Rome, Italy, 1954; Volume 36, pp. 216–219.
60. Melton, M.A. *An Analysis of the Relations among Elements of Climate, Surface Properties, and Geomorphology*; Technical Report No. 11; Columbia University, Department of Geology, Office of Naval Research: New York, NY, USA, 1957.
61. Horton, R.E. Drainage-basin characteristics. *EOS Trans. Am. Geophys. Union* **1932**, *13*, 350–361. [CrossRef]
62. Potter, P.E. A Quantitative Geomorphic Study of Drainage Basin Characteristics in the Clinch Mountain Area, Virginia and Tennessee. V. C. Miller. *J. Geol.* **1957**, *65*, 112–113. [CrossRef]
63. Strahler, A.N. Quantitative analysis of watershed geomorphology. *Eos Trans. Am. Geophys. Union* **1957**, *38*, 913–920. [CrossRef]
64. Strahler, A.N. Hypsometric (area-altitude) analysis of erosional topography. *Bull. Geol. Soc. Am.* **1952**, *63*, 1117–1142. [CrossRef]
65. Wood, W.F.; Snell, J.B. *A Quantitative System for Classifying Landforms*; Technical Report EP-124; U.S. Army Quartermaster Research and Engineering Center: Natick, MA, USA, 1960.
66. Church, M.; Mark, D.M. On size and scale in geomorphology. *Prog. Phys. Geogr.* **1980**, *4*, 342–390. [CrossRef]
67. Wilson, M.F.J.; O'Connell, B.; Brown, C.; Guinan, J.C.; Grehan, A.J. Multiscale terrain analysis of multibeam bathymetry data for habitat mapping on the continental slope. *Mar. Geod.* **2007**, *30*, 3–35. [CrossRef]
68. Beven, K.J.; Kirkby, M.J. A physically based, variable contributing area model of basin hydrology. *Hydrol. Sci. Bull.* **1979**, *24*, 43–69. [CrossRef]
69. Moore, I.D.; Grayson, R.B.; Ladson, A.R. Digital terrain modelling: A review of hydrological, geomorphological, and biological applications. *Hydrol. Process.* **1991**, *5*, 3–30. [CrossRef]
70. Hoek, E.; Brown, E.T. Practical estimates of rock mass strength. *Int. J. Rock Mech. Min. Sci.* **1997**, *34*, 1165–1186. [CrossRef]
71. Brideau, M.-A.; Yan, M.; Stead, D. The role of tectonic damage and brittle rock fracture in the development of large rock slope failures. *Geomorphology* **2009**, *103*, 30–49. [CrossRef]
72. Xie, H.; Dong, J.; Shen, Z.; Chen, L.; Lai, X.; Qiu, J.; Wei, G.; Peng, Y.; Chen, X. Intra- and inter-event characteristics and controlling factors of agricultural nonpoint source pollution under different types of rainfall-runoff events. *Catena* **2019**, *182*, 104105. [CrossRef]
73. Xu, X. Chinese Population Spatial Distribution Kilometer Grid Data Set. Available online: http://www.resdc.cn/DOI (accessed on 20 November 2021).
74. Lin, H.-M.; Chang, S.-K.; Wu, J.-H.; Juang, C.H. Neural network-based model for assessing failure potential of highway slopes in the Alishan, Taiwan Area: Pre- and post-earthquake investigation. *Eng. Geol.* **2009**, *104*, 280–289. [CrossRef]
75. Chang, S.-K.; Lee, D.-H.; Wu, J.-H.; Juang, C.H. Rainfall-based criteria for assessing slump rate of mountainous highway slopes: A case study of slopes along Highway 18 in Alishan, Taiwan. *Eng. Geol.* **2011**, *118*, 63–74. [CrossRef]
76. Guyon, I.; Weston, J.; Barnhill, S.; Vapnik, V. Gene selection for cancer classification using support vector machines. *Mach. Learn.* **2002**, *46*, 389–422. [CrossRef]

77. Li, X.; Wang, Y.; Basu, S.; Kumbier, K.; Yu, B. A Debiased MDI Feature Importance Measure for Random Forests. In Proceedings of the 33rd Conference on Neural Information Processing Systems (NeurIPS 2019), Vancouver, BC, Canada, 8–14 December 2019.
78. Dietrich, A.; Krautblatter, M. Evidence for enhanced debris-flow activity in the Northern Calcareous Alps since the 1980s (Plansee, Austria). *Geomorphology* **2017**, *287*, 144–158. [CrossRef]
79. Liang, Z.; Wang, C.; Ma, D.; Khan, K.U.J. Exploring the potential relationship between the occurrence of debris flow and landslides. *Nat. Hazards Earth Syst. Sci.* **2021**, *21*, 1247–1262. [CrossRef]
80. Iverson, R.M.; Reid, M.E.; LaHusen, R.G. Debris-flow mobilization from landslides. *Annu. Rev. Earth Planet. Sci.* **1997**, *25*, 85–138. [CrossRef]
81. Li, J.; Wang, X.; Jia, H.; Liu, Y.; Zhao, Y.; Shi, C.; Zhang, F.; Wang, K. Assessing the soil moisture effects of planted vegetation on slope stability in shallow landslide-prone areas. *J. Soils Sediments* **2021**, *21*, 2551–2565. [CrossRef]
82. Li, K.; Yue, D.; Guo, J.; Jiang, F.; Zeng, J.; Zou, M.; Segarra, E. Geohazards mitigation strategies simulation and evaluation based on surface runoff depth: A case study in Bailong River basin. *Catena* **2019**, *173*, 1–8. [CrossRef]
83. Shen, P.; Zhang, L.M.; Chen, H.X.; Gao, L. Role of vegetation restoration in mitigating hillslope erosion and debris flows. *Eng. Geol.* **2017**, *216*, 122–133. [CrossRef]
84. Balzano, B.; Tarantino, A.; Ridley, A. Preliminary analysis on the impacts of the rhizosphere on occurrence of rainfall-induced shallow landslides. *Landslides* **2019**, *16*, 1885–1901. [CrossRef]
85. Shen, P.; Zhang, L.M.; Fan, R.L.; Zhu, H.; Zhang, S. Declining geohazard activity with vegetation recovery during first ten years after the 2008 Wenchuan earthquake. *Geomorphology* **2020**, *352*, 106989. [CrossRef]
86. Wang, S.; Meng, X.; Chen, G.; Guo, P.; Xiong, M.; Zeng, R. Effects of vegetation on debris flow mitigation: A case study from Gansu province, China. *Geomorphology* **2017**, *282*, 64–73. [CrossRef]
87. Zhao, Y. DF_distribution.zip. Available online: http://dx.doi.org/10.13140/RG.2.2.11129.19048 (accessed on 20 November 2021).